Electronic characterization of supramolecular materials at the nanoscale by Conductive Atomic Force and Kelvin Probe Force microscopies

Chiara Musumeci[1,3], Andrea Liscio[2,3], Vincenzo Palermo[2,*] and Paolo Samorì[1,*]

[1] Nanochemistry Laboratory, ISIS & icFRC, Université de Strasbourg & CNRS, 8 allée Gaspard Monge, 67000 Strasbourg, France
[2] Istituto per la Sintesi Organica e la Fotoreattività – Consiglio Nazionale delle Ricerche, via Gobetti 101, 40129 Bologna, Italy

The performances of organic (opto)electronic devices strongly depend on the order at the supramolecular level. Unraveling the relationship between structural and electronic properties in nanoscale architectures is therefore key for both fundamental studies and technological applications. C-AFM and KPFM provide an immediate correlation between the morphology of a material and its electrical/electronic properties such as local conductivity and surface potential. Thus, they are unrivaled techniques offering crucial information toward the optimization of the real devices, ultimately providing an important contribution to a hot field at the cross-road between nanoscience and organic (opto)electronics. Herein we focus on the application of C-AFM and KPFM on self-assembled monolayers (SAMs), organic (semi)conducting materials for thin film transistors (TFTs) and organic blends for photovoltaics (OSCs).

Introduction

Materials based on conjugated polymers and small molecules exhibit well-defined optical and electrical properties, making them ideal active components in opto-electronic devices such as light-emitting diodes, field-effect transistors and solar cells [1–3]. These basic devices can be used to develop flexible displays, smart windows, sensors, memories, etc. with the promise of low-cost manufacturing [4]. It is however notorious that these materials possess nanoscale heterogeneities in their optical and electrical properties that affect the device performances. These heterogeneities arise from structural and morphological features that vary as a function of the type of chosen molecule and substrate, film processing and device fabrication conditions [5,6]. Structural factors such as amorphous regions, grain boundaries, and local defects within crystalline domains or phase segregated blends have been shown to directly correlate with the opto-electronic properties of these organic materials and more specifically with charge carrier mobility in field-effect transistors, or efficiency in solar cells [7–11]. The characterization of these structural defects, which are responsible for a lowering of the performance, is therefore an important goal of organic opto-electronics. Characterization techniques based on light–matter interactions, ranging from optical spectroscopy to X-ray based techniques, have been largely used to correlate the structure of organic materials to their charge transport characteristics, and are being constantly improved in terms of spatial and energetic resolution [12,13]. However, the smallest area that is probed in a single measurement done with these techniques amounts to some mm [2], thus the obtained signals are averaged out of an Avogadro number of molecules. Scanning probe microscopies (SPM) offer unrivaled insights into these issues by providing a high-resolution direct view of the thin films morphology, size and orientation of crystalline domains or grain boundaries on the nanometer scale [14,15]. Electrical SPM modes [16] are particularly appropriate since they give an immediate correlation between the morphology of a material and its electric properties [17,18] such as local conductivity (by Conductive Atomic Force Microscopy, C-AFM) [19] and surface potential (by Kelvin Probe Force Microscopy, KPFM) [20,21]. The former provides a direct access to the intrinsic electrical properties at the nanoscale by measuring the current flowing between the tip and the conductive sample. The latter makes it possible to monitor the electrical potential even in working devices. These two techniques are highly complementary: C-AFM is

*Corresponding authors:. Palermo, V. (vincenzo.palermo@isof.cnr.it), Samorì, P. (samori@unistra.fr)
[3] These authors equally contributed to this work.

1369-7021/© 2014 Elsevier Ltd. All rights reserved. http://dx.doi.org/10.1016/j.mattod.2014.05.010

based on charge transport between the sample and the tip when they are at close distance. It needs a very efficient physical contact between tip and sample, thus perturbing to a certain extent the sample by mechanical pressure and charge injection. Conversely, KPFM is a contactless technique, based on long-ranged electrostatic interactions, with no mechanical action of the tip on the sample. Even electric perturbation of the sample is minimal because the instrument tries to match the potential of the tip with the one of the sample, thus minimizing any electrostatic interaction between the two.In this review we highlight recent works performed by making use of C-AFM and KPFM with the aim of getting fundamental information on the nanoscale electrical and electronic properties of organic and supramolecular materials effectively employed as active layers as real opto-electronic devices. After a brief description of the two scanning probe modes, this article describes the nanoscale resolved electrical characterization of molecular self-assembled monolayers (SAMs) on solid surfaces relevant for technological applications. These SAMs are key since they enable the tuning of the energetics at the interfaces, and are also important model systems for investigating the conduction mechanisms along single molecules. Then, we describe how SPM can be used to map the morphology of thin films and to detect the electrical properties of high performing organic (semi)conducting materials integrated Organic Thin-Film Transistors (OTFT). Finally, we describe the electrical nanoscale characterization of Organic Photovoltaics (OPVs) materials, with a particular focus on bulk hetero-junctions (BHJ), when tested under an additional stimulus, that is, light. We conclude our overview by discussing some outlooks and future developments of these two techniques.

Techniques

C-AFM and KPFM can be considered being modes of Atomic Force Microscopy (AFM) since they are typically operating on the very same set-up. A microfabricated cantilever exposing at its edge a sharp metal or metal-coated tip is used to sense the surface and to map both its morphology and its electrical features. The tip is scanned over the surface and its position is mapped by monitoring a laser beam reflected from the backside of the cantilever into a photodetector (Fig. 1a–c). By sensing different electrical signals, the two techniques operate on two opposite regimes: in C-AFM the tip is in physical contact with the sample to allow measurements of the flowing current (Fig. 1d), whereas in KPFM the tip passes over the surface without being in direct contact with it (Fig. 1e).

In C-AFM a feedback loop is used to move the probe along the *Z*-axis in order to maintain a constant cantilever deflection *z* (Fig. 1f); considering the cantilever as a perfect spring, a controlled constant force F is therefore exerted by the tip on the sample surface according to Hooke's law ($F = k \cdot z$), where k is the spring stiffness. As a result, the tip follows the contour of the sample surface and provides a map of the surface topography. Simultaneously, a voltage is applied between the conductive tip, acting as a movable electrode, and a counter-electrode, and the resulting current is measured. In this way a direct correlation between the nanoscale structure and local electric conductivity becomes possible. In case of studies of very soft and fragile materials a different method can be employed, named *Torsional Resonance Tunneling Atomic Force Microscopy* (*TR-TUNA AFM*). In this mode the tip oscillates laterally with respect to the sample surface, being in this way continuously kept in the near field to enable the measurement of tunneling currents [22,23]. In the simplest configuration the organic material is deposited on top of a conductive substrate and the conductive tip is scanned over such a surface (Fig. 1a) by measuring point by point the current flowing vertically. Conversely, in a horizontal configuration the organic material is deposited on an insulating support and the electrical connection is obtained by laterally patterning a metal electrode (Fig. 1b). Current can in this way flow through the organic layer, from the biased lateral contact to the movable metal-coated scanning probe tip. Fig. 1c portrays a configuration named *photoconductive-AFM* (*PC-AFM*): it exploits a light source to excite the sample, and the resulting photocurrent is measured by the AFM probe.

Differently from C-AFM, the KPFM does not measure a current flow but rather the surface potential (SP) of the sample by recording the electrostatic forces resulting from the interaction between tip and sample. Electrostatic forces, being a long-ranged interaction, do not require a physical contact between the two bodies. KPFM is in fact a non-contact AFM technique based on Zeeman vibrating capacitor set-up where the two electrodes of the capacitor are the sample and an oscillating conductive AFM tip (with defined frequency ω_0). During the KPFM scan, both an AC- and DC-bias are simultaneously applied to the tip and the first harmonic of the resulting tip-sample capacitive force is $F_{\omega 0} = V_{AC} \cdot (V_{DC} - \Delta SP)(dC/dz)$, where ΔSP is the surface potential difference between tip and sample fixed at z distance, while C is the total capacitance of the system. The feedback circuit is used to nullify the first harmonic term by tuning $V_{DC} = \Delta SP$.

To minimize a possible cross talk between the topography and the electrostatic signal is commonly used the ''two-pass technique'' configuration (i.e. Lift Mode). KPFM image is obtained by rastering the surface at fixed tip-sample distance [24]. Each line is scanned twice where the short-range van der Waals forces between tip and sample is tuned by varying the tip-sample distance. In the first scan the topography of the surface is determined (AFM scan), and during the second scan the tip is raised up to a fixed distance (i.e. lift height) above the sample surface (see Fig. 1g). For each tip position the active feedback provides to nullify the $F_{\omega 0}$ term by detecting the amplitude oscillation of the tip which is equal to zero when $V_{DC} = \Delta SP$. A comprehensive description can be found in [25,26] and references therein.

In general, the lateral resolution strongly depends on the geometry of the tip-sample system [27,28]. The large tip-sample distance (typically in the range of 10–100 nm) and the long-ranges electrostatic forces limit the lateral resolution of the technique to few tens of nm.

The physical meaning of the measured surface potential is strictly related to the sample and its electrical properties. In the case of metallic samples, the measured surface potential corresponds to the work function difference between tip and sample. This definition can be generalized for SAMs and thin films. In the former case it is common to define an effective work function as the sum of the substrate work function and the SAM dipole moment [29]. In the latter case, other additional terms should be taken into account such as interface dipoles, band bending and the presence of fixed charges. Moving from metallic to semiconducting or even insulating samples, SP is not directly correlated to the work function anymore, but is instead influenced by local charge density [30].

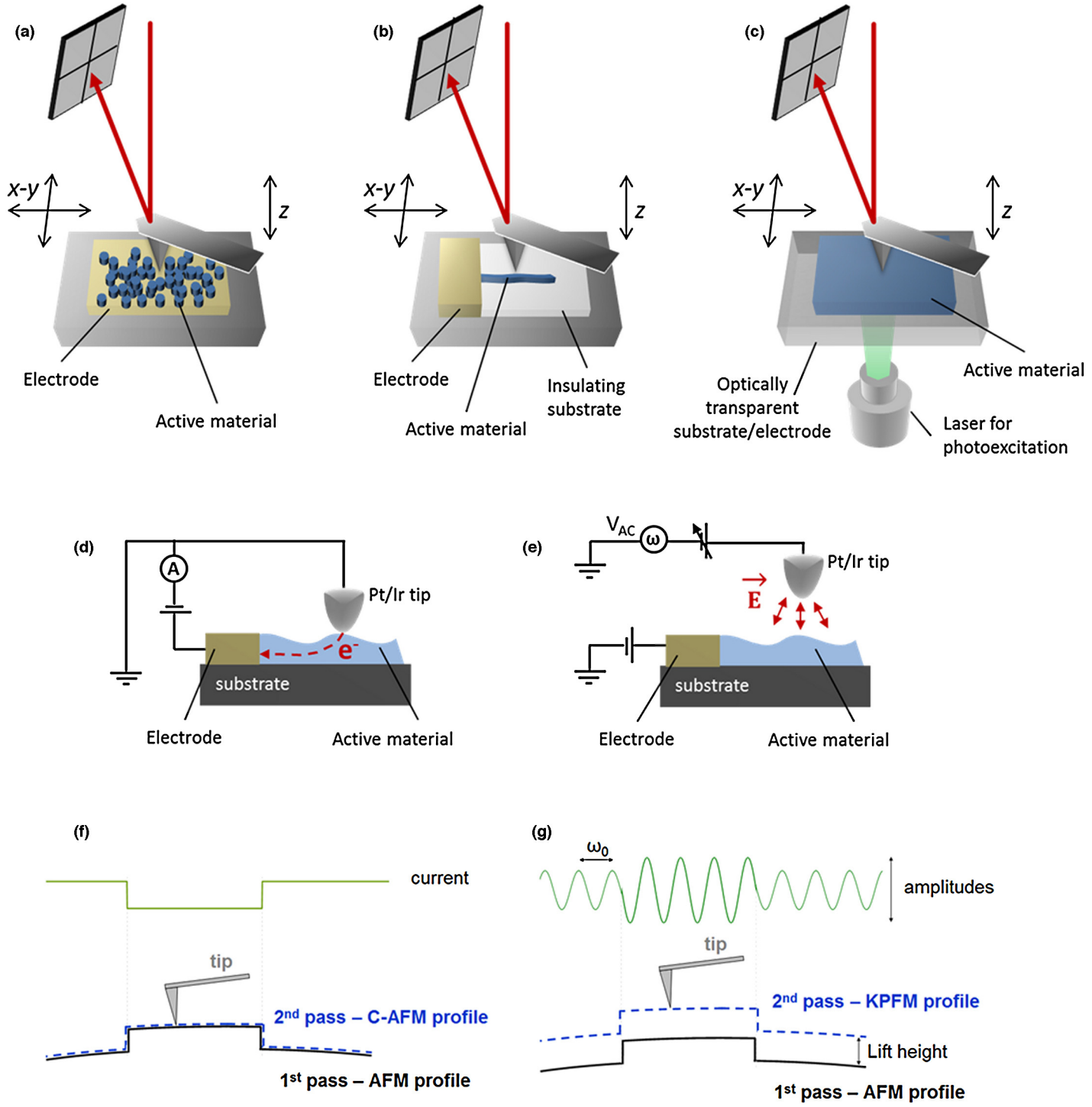

FIGURE 1

Cartoons showing the different setups: SPMs in (a) vertical and (b) horizontal configuration, (c) photoconductive SPM. (d), (f) C-AFM operating in contact mode and corresponding scheme, (e), (g) KPFM operating in non-contact mode and the corresponding scheme.

Self-assembled monolayers

Chemisorbed SAMs are structurally well-defined architectures exhibiting tunable physical and chemical surface properties thereby providing a convenient, flexible, and simple solution to tailor the interfacial properties of metals, metal oxides, and semiconductors [31]. In particular, molecules exposing thiol and silane moieties are prone to chemisorb on metal and dielectric surfaces, respectively, and because of this reason they are being frequently used for surface modification in molecular [32] and organic electronics [9]. In general, the formation of a SAM on metals strongly modifies not only its hydrophobic/hydrophilic nature to promote the formation of structurally improved metal–semiconductor interfaces, but also the effective work function of the surface due to the presence of oriented molecules possessing an intrinsic dipole. Because of these reasons the growth of suitable SAMs on metal electrodes is used to improve charge injection at metal–semiconductor interfaces.

The adsorption of molecules on conducting electrodes can be used as a way to modify their work function, as studied with KPFM

by Nikiforov et al. [33] on ultra-thin films of porphyrin evaporated on highly oriented pyrolytic graphite (HOPG). When the porphyrin ring is oriented parallel to the substrate, the surface work function is 50 mV less than that of the HOPG; in contrast, when the porphyrin molecular plane is oriented perpendicular to the substrate, the work function of the surface is unchanged, that is, it matches that of HOPG. This orientation dependence of the surface work function derives from the degree of overlap of the frontier orbital of the molecule with the Fermi level of the conducting substrate.

Molecules decorated with thiol end-groups are known to form SAMs on metals belonging to group Ib and group VIII. They rely on the formation of stable covalent bonds between the substrate atoms and the sulphur moiety (the energy of Au-S chemical bond amounts to 40 kcal/mol). The so-obtained surface exhibits tailor-made properties. By using Ultraviolet Photoemission Spectroscopy (UPS), Alloway et al. [34] showed that the work function of Au(111) surface can be modified in a range of 1.6 eV by chemisorption of different alkanethiols and partially fluorinated alkanethiols SAMs. By comparing the values measured by Alloway for the different chain lengths, it appears that the effective work function of the system varies linearly with the molecular length by 20 ± 8 meV per CH_2 unit. This result was ascribed to the changing dielectric behavior of the hydrocarbon tail region and to the dipole of the fluorinated substitution. In general, UPS and macroscopic Kelvin Probe were the most commonly used techniques to quantify the effective work function of SAM on metallic surfaces. Since the '90s KPFM has been employed to explore the electronic properties of phase-separated SAMs made with different alkanethiols on Au(1 1 1) with a lateral and potential resolution of a few tens of nm and 5 meV, respectively. These investigations revealed a linear dependence of the effective work function with the molecular length by 14 ± 3 meV per CH_2 unit measured by Lu et al. [35], in good accordance with the values obtained by UPS. It is noteworthy to highlight that effective WF values measured by KPFM are affected by the experimental artifacts of the technique those are responsible for the underestimation of the measured potential. Different papers report lower WF values measured on the same systems because of the size of investigated SAM amounts few hundreds of nm. Also in the case of Lu et al., although the size of the investigated SAM structures amounts to about 1 μm, an underestimation of about 15% has to be taken into account due to an incorrect use of the histogram analysis of acquired potential values (see [36] for more details).

The work function variation depends on the density and the packing of the chemisorbed thiolated molecules [39], which increases with the crystallinity of the Au surface [40]. Electrochemical impedance studies [41,42] demonstrated that Au electrodes modified by long alkyl SAMs exhibit electron transfer at pinholes and electron tunneling at defects, both processes occurring between the electrolytic solution and the SAM-coated gold electrodes. Moreover, parameters as quality, stability and compactness of SAMs do not only depend on the physical and chemical structure of the constituting molecules and on the nature of the molecule–surface interaction, but also on the cleanliness of the electrode surface and mode of preparation. Liscio et al. [37] used KPFM to monitor the preparation of asymmetric electrodes with alkanethiol SAMs with different chain lengths (i.e. dodecanethiol and hexanethiol) using selective electrochemical desorption on interdigitated source–drain electrodes with 200 nm gap. KPFM measurements provided direct quantitative mapping of the WF of the coated electrodes making it possible to identify the interdigitated electrodes covered by alternating dodecanethiol and hexanethiol monolayers (Fig. 2a–c).

Thiol functionalized molecules exposing stimuli-responsive moieties have been employed to realize switchable interfaces that can reversibly modify the physical and chemical properties of gold electrodes as a result of external stimuli. The photo-triggered isomerization between *trans* and *cis* isomer in azobenzenes forming a SAM has been exploited to modify the effective work function of the electrode by simply exposing the film to UV light. By comparing results obtained using four experimental techniques (KPFM, macroscopic Kelvin Probe, electroabsorption and ultraviolet photoelectron spectroscopy) Crivillers et al. [43] showed that in the case of azo-biphenyl SAMs, the work function shift induced by the photoisomerization does not depend on the type of gold substrate employed. In fact, both on films chemisorbed on Au(1 1 1) or on polycrystalline commercial micro-electrodes, the measured work function change amounts to 120 ± 10 meV and a complete reversible *trans–cis* switching is observed. Similar behaviors have been observed on SAM of thiolated azobenzene molecule with a perfluorinated benzene head group [44], confirming the robustness of the chemical switch of the azobenzene-SAM. Its technological relevance has been proved by exploiting the photo-responsive nature of the azobenzene SAMs chemisorbed on Au electrodes in order to modulate the charge injection at a metal–semiconductor interface, thereby fabricating a prototype of optically switchable organic field-effect transistor [45].

Silanes are chemical groups possessing a hydrolytically sensitive center that can react with inorganic substrates such as glass, silicon, silicon oxide and as well as organic semiconducting substrates thereby affecting their hydrophobic/hydrophilic nature. Among them, hexamethyldisilasane (HMDS), octadecyltrimethoxysilane (OTMS) and octyltrichlorosilane (OTS) SAMs [46,47] are commonly used to passivate the SiO_2 surfaces in order to prevent the water-related charge trapping at semiconductor/dielectric interface in electrical devices. By using KPFM to visualize in real time the potential decay in the gap between source and drain electrodes, Mathijssen et al. [48] monitored the dynamics of trapping and detrapping of charges on bare and HMDS passivated SiO_2, clearly demonstrating that the commonly observed bias-stress effect in OFETs is mainly due to water charge trapping on the SiO_2 surface.

By using rubrene single crystal surfaces functionalized with OTS, Ellison et al. [38] determined the type and degree of interfacial charge-transfer doping caused by the SAM molecules by measuring SAM-induced surface potential changes (Fig. 2). They quantified the amount of the SAM-induced surface potentials on rubrene single crystals by partially coating them with OTS SAMs, and measuring the type and degree of interfacial charge-transfer doping caused by the SAM molecules. The measured SP value corresponds to the difference between the vacuum level (E_{VAC}) and the work function of the tip (E_F) corresponding to eV_P and eV_n for *p*-doped and pristine substrates, respectively. The SAM induces a *p*-type chemical doping of rubrene, because the Fermi level (E_F) shifts very near to the HOMO band (E_H). For the sake of simplicity, a complete scheme of the energetics is displayed in the Fig. 2f

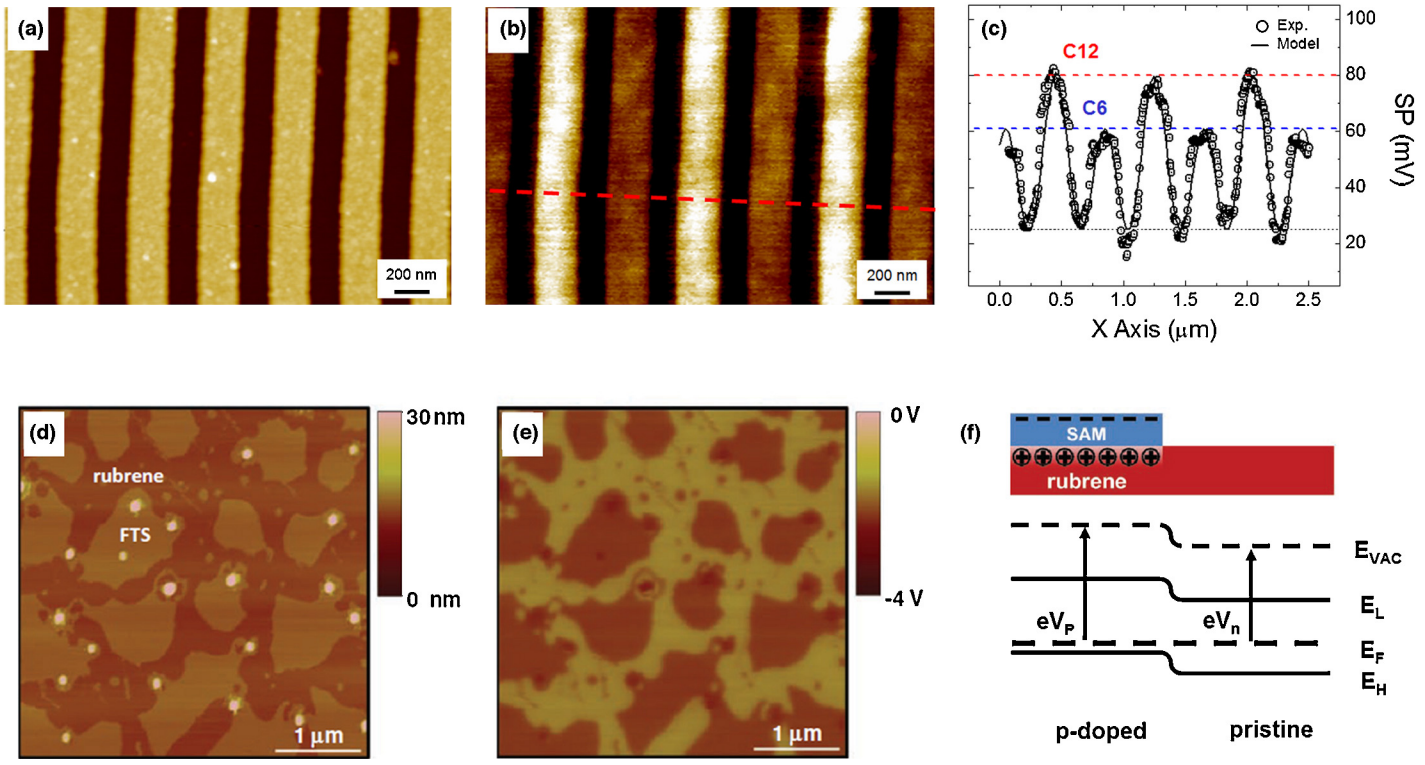

FIGURE 2

(a) Topography and (b) surface potential image of nanometric source–drain interdigitated electrodes covered by alternating dodecanethiol and hexanethiol monolayers. (c) Surface potential profile (circles) taken along the red line in b. Reproduced from [37] with the permission of Wiley-VCH. (d) Topography and (e) the corresponding surface potential maps of rubrene partially coated with FTS SAM. (f) Scheme of energetic levels of rubrene/SAM heterostructure. *Z*-range: (a) 100 nm, (b) 80 mV. Reproduced from [38] with the permission of Wiley-VCH.

reporting also the LUMO band (E_L). Since KPFM allows one to explore simultaneously morphology and surface potential of nanostructured films, it was used to study the SAM nucleation and growth process with the ultimate goal of understanding the impact of microstructure and adsorbates on the electrical properties.

Following the seminal C-AFM work by Wold and Frisbie exploring the local current–voltage properties on alkanethiol SAMs covalently grown on Au(1 1 1) [49], C-AFM became a popular tool to characterize the resistivity of SAMs chemisorbed on conductive substrates. By studying the dependence of the conductivity on the molecular length C-AFM gives valuable information on the charge transport along a molecular wire. Since the mechanism responsible for charge transport in these cases is tunneling, measuring the current decay factor β is a suitable method to describe and compare the electrical characteristics of different molecular systems. As a result, many alkanethiols, alkanedithiols, and alkylamines molecules have been investigated by C-AFM, most of them revealing β values in the range 0.7–1 $Å^{-1}$ [19].

The conductivity of SAMs made with π-conjugated molecules has been the subject of many experimental and theoretical investigations because of the better capability of conjugate systems to transport charges though longer distances. Because of this reason, rigid conjugated molecules have attracted a lot of interest because of their potential technological application as molecular wires. Accordingly, lower tunneling decay factors have been measured with respect to non-conjugated molecules of comparable lengths [50]. Average β values of 0.42 ± 0.07 $Å^{-1}$ were determined for example for oligophenylene thiolate SAMs, to be compared to the $\beta = 0.94 \pm 0.06$ $Å^{-1}$ for alkanethiolate SAMs on the same length [50]. When site-specific disruption of conjugation is introduced via chemical design, higher resistances are measured compared to the equivalent fully conjugated wire [51,52].

The junction resistance is also strongly affected by the type of head group used to tether the molecule to the electrode surface. For rigid conjugated oligoacenes with a contour length ranging from one to four aromatic rings (0.8–1.5 nm in length), the β was estimated being 0.5 $Å^{-1}$ for the monothiol- and 0.2 $Å^{-1}$ for the corresponding dithiol-capped. The contact resistance (R_0) was 10–100 times lower for dithiol junctions, indicating that chemical contacts reduce both the tunneling barrier height and contact resistance significantly [53]. When different metal substrates are employed it was shown that the β values are independent of their work function, while R_0 exhibited strong work function dependence [54].

The possibility to employ conjugated molecules as molecular wires to transport the current over long distances has led to the engineering of new molecular systems that can be grown up to tens of nanometers in length in a controlled manner. Oligophenyleneimine (OPI) [51], oligonaphthalenefluoreneimine (ONI) [52] and donor/acceptor oligo-tetrathiafulvalene-pyromelliticdiimide-imine (OTPI) [55] wires, with lengths ranging from 1 to 7–20 nm, have been synthesized and linked on gold surfaces. Local current–voltage *I–V* characteristics performed by C-AFM in vertical configuration made it possible to observe the theoretically predicted change in charge transport from tunneling to hopping as a function of the wire length.

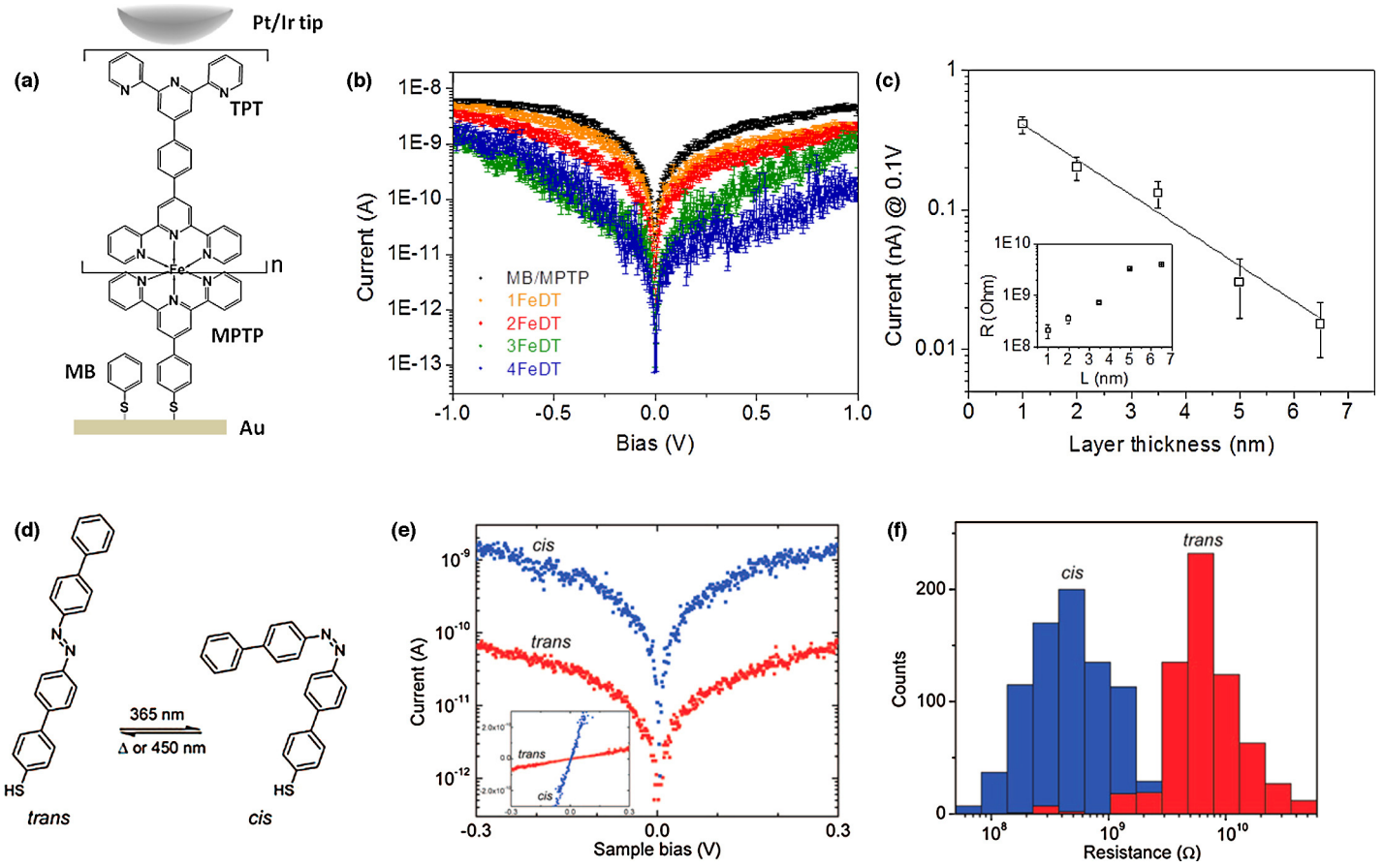

FIGURE 3

(a)–(c) Length dependent conductance measurements performed on Fe-bis(terpyridine) molecular wires grown on gold by layer-by-layer assembly, showing a clear scaling of the current with for the subsequent coordination steps. The plots of the current at low bias (c) as well as the low voltage resistance (inset) as functions of the layer thickness allowed the estimation of a very low current attenuation. Reproduced from [56] with the permission of Wiley-VCH. (d) Molecular switch based on thiolated azobenzene designed to be chemisorbed on Au(1 1 1) surfaces. (e)–(f) Photoinduced conformational change in bis(diphenyl)-azobenzene molecules showed a 30-fold decrease in resistance when going from the *trans* to the *cis* state, as shown by the average *I–V* curves (e) and by the low bias resistance distributions (f). Reproduced from [57] with the permission of ACS.

Recently we exploited metallo-ligand interactions to grow Fe-bis(terpyridine) based ordered nanostructures of desired length on gold support by layer-by-layer assembly. The experimental length dependent conductance measurements performed by C-AFM, showed in Fig. 3a–c, corroborated by theoretical calculations, provided unambiguous evidence for the existence of a hopping charge transport mechanism, characterized by a very low current attenuation ($\beta = 0.058 \pm 0.006$ Å^{-1}) and a regime transition from Ohmic conduction to SCLC at higher bias [56].

Additionally to the studies of SAMs conductivity in dependence of their molecular lengths, another technique is becoming popular, named transition voltage spectroscopy [58]. It involves the analysis of the current–voltage curves at higher bias. An inflection point on a Fowler–Nordheim plot, that is, a $\ln(I/V^2)$ vs. $(1/V)$ plot, for short wires having $L < 3$–4 nm, is consistent with a change in the transport regime from direct tunneling to field emission. The voltage (V_{trans}) at which this transition occurs was found to depend linearly on the energy offset between the metal Fermi level and molecular energy levels [59]. Since the magnitude of V_{trans} is independent on the contact area, information on the effective barrier height of a molecule can be garnered without possessing a specific knowledge of the number of molecules in the junction. Moreover, by looking at the dependence of the V_{trans} on the work function of the metal it is also possible to discriminate between a HOMO-mediated transport (hole tunneling) or a LUMO-mediated one (electron tunneling) thereby providing information on the dominant charge carrier [60].

In addition to the metal-molecule energy differences caused by the molecular structure (π- or σ-bond), charge transport through molecules is also greatly influenced by the conformations and configuration that the molecules adopt on the solid support. Monolayers consisting of photochromic molecules undergoing a light-induced isomerization can behave as molecular switches. The direct immobilization of diarylethene having an acetylene moiety onto a on hydrogen-terminated Si(1 1 1) surfaces using a thermal hydrosilylation reaction gave an approximately 2-fold increase in current when going from the *open* form to the *close* one [61]. Similarly, two different conductance states have been measured in azobenzene-based SAMs have been detected depending on the present isomeric form (*trans* or *cis*). The current in nanoscopic molecular junctions incorporating bis(diphenyl)-azobenzene molecules showed a 30-fold decrease in resistance when going from the *trans* to the *cis* state [57], as the result of a decrease in tunneling barrier length associated with the

molecular conformational change (see Fig. 3d–f). An even higher photoinduced I_{on}/I_{off} ratio up to 7×10^3 between the *cis* and *trans* configurations was found on azobenzene–bithiophene derivatives linked to gold [62] and attributed to a synergic combination of SAM thickness variation and modification of the energy offset between the lowest unoccupied molecular orbital (LUMO) and the electrode Fermi energy [62].

The possibility of C-AFM of controlling the load force exerted by the tip on the molecular junction has also allowed studying the effect of an applied force on the electrical properties of a material at the nanoscale. For example it allows to gain insight into the dependence of the electrical transport on the tilt angle of molecules adsorbed on a surface. It was shown that by increasing tilt angle, alkanethiol SAMs exhibit improved intermolecular charge transfer. In fact, as the molecular tilt angle increases with the tip-loading force, the chain-to-chain tunneling becomes significant, in addition to the already existing through-bond tunneling in overall transport [63]. Moreover, the onset for Fowler–Nordheim tunneling (V_{trans}) shifts to lower voltages as the tip loading force is augmented, increasing the tilt angle, as a result of an enhancement of field emission due to a barrier thinning and consequently increasing electric field [64].

It is worth stressing that reliable current–voltage measurements on SAMs require collection of a large set of data to be analyzed using statistical tools. One of the first systematic approach employed molecules of 1,8-octanedithiol which were inserted into an octanethiol monolayer on Au(1 1 1) using a replacement reaction. The thiol groups at the top of the film were used to bind gold nanoparticles. This allowed locating individual nanoparticles and to contact them with the AFM tip. Current–voltage curves were then quantized as integer multiples of one fundamental curve to identify single-molecule contacts [65]. Similar approaches have also been reported to evaluate single molecule conductivity by C-AFM break-junction measurements [66–69]. Recently, a different approach was proposed [70] employing large arrays of sub-10 nm single crystal Au nanodots electrodes on silicon substrate. Each nanodot was covered by the SAM of interest and the C-AFM tip was scanned over the whole array at a fixed voltage. By analyzing the current map images with a thresholding program, the authors were then able to reconstruct conductance histograms referred to thousands of junctions. Another methodology consisted in building up two-dimensional histograms by logarithmically binning the *dI/dV* values, determined numerically from thousands of *I–V* curves, for each voltage applied. This method made it possible to distinguish general tendencies in the *dI/dV* curves from statistical variations in the conductance values, making it possible to recognize destructive quantum interference effects in the transport of cross conjugated molecular wires compared to the corresponding linearly conjugated ones [71].

A number of variables are known to strongly affect C-AFM measurements such as substrate roughness, tip chemistry, presence of solvent, extensive tip usage, applied load and tip radius [72]. The issue of stability and reproducibility has certainly a huge importance when absolute values are needed in order to estimate the intrinsic electric properties of a single molecular layer. The problem can be tackled by exploring a large numbers of junctions in order to get reliable statistics. However, since C-AFM is a pretty slow technique, a sound statistical analysis is extremely time demanding. All the methods introduced in the paragraph above not only have to cope with this issue, but are also pretty sophisticated thus not commonly achievable using standard equipped laboratories. In light of this future effort should be devoted to devise rigorous but at the same time simplified procedures that can offer a statistical treatment of huge amount of data, in order to make the technique more easily accessible.

When studying the electrical behavior of SAMs, one has to take into account that beyond the intrinsic properties of the molecules, an important role is played by the chosen metal electrode and by the molecule–electrode coupling. The use of different chemical groups able to covalently bind a molecule to a metal surface, beyond the most common thiol moiety, and/or electrodes possessing different work functions could further improve the understanding of the transport across molecular nanojunctions.

Organic (semi)conducting materials for thin film transistors (TFTs)

In a SAM the charge transport is typically a through bond process, although a contribution of a through-space conduction cannot be ignored a priori, especially when the tilt angles of molecules at surfaces is high (see the above paragraphs); because of this reason C-AFM is a precious tool for studies on SAMs in order to get insights into the conduction mechanisms responsible for charge transport along the single molecules. Conversely, in macroscopic devices the overall electrical properties depend on how the single building blocks (i.e. either single molecules, crystalline domains or mesoscopic structures) assemble together.

A lateral transport governed by the interconnection among individual fullerene molecules was recently measured by Bassani and co-workers by growing a fullerene terminate SAM covalently linked to SiO_2. The resistance between the C-AFM tip contacting the SAM and a patterned counter electrode was determined. The charge transport, which was detected up to 1.5 μm away from the electrode, appears to be intrinsically space-charge limited, and governed by the connectivity of the fullerene clusters [73]. Lateral transport was also probed in oligothiophene Langmuir–Blodgett monolayer islands deposited on native oxide-covered Si-p^+ bottom electrode. Because of the larger resistance associated with the oxide layer with respect to that between the molecules, the current was found to depend linearly on the island diameter as a result of an increase contact area. Moreover, the transport in a single grain was found to occur preferentially in one direction, corresponding to the direction where π-orbitals of the thiophene units overlap more [74]. Already in the late '90s, Frisbie et al. had assessed the horizontal electrical transport of single sexithiophene (6T) grains both in two and three terminal devices at the nanoscale, also estimating the resistance at one single grain boundary (Fig. 4a) [75–78]. The interconnection among crystalline domains was shown to drastically affect charge transport also in polycrystalline organic semiconducting thin films [79,80], so that understanding the nature of these boundaries and how they influence charge transport is critical to the field of organic electronics. Spherulites, that is, structures arising from a single nucleation point and including a distribution of orientations around the radial axis, are frequently observed in polycrystalline solution-processed organic semiconductor thin films, such as triethylsilylethynyl anthradithiophene (TES ADT). The boundaries between neighboring spherulites exhibit varying angles of

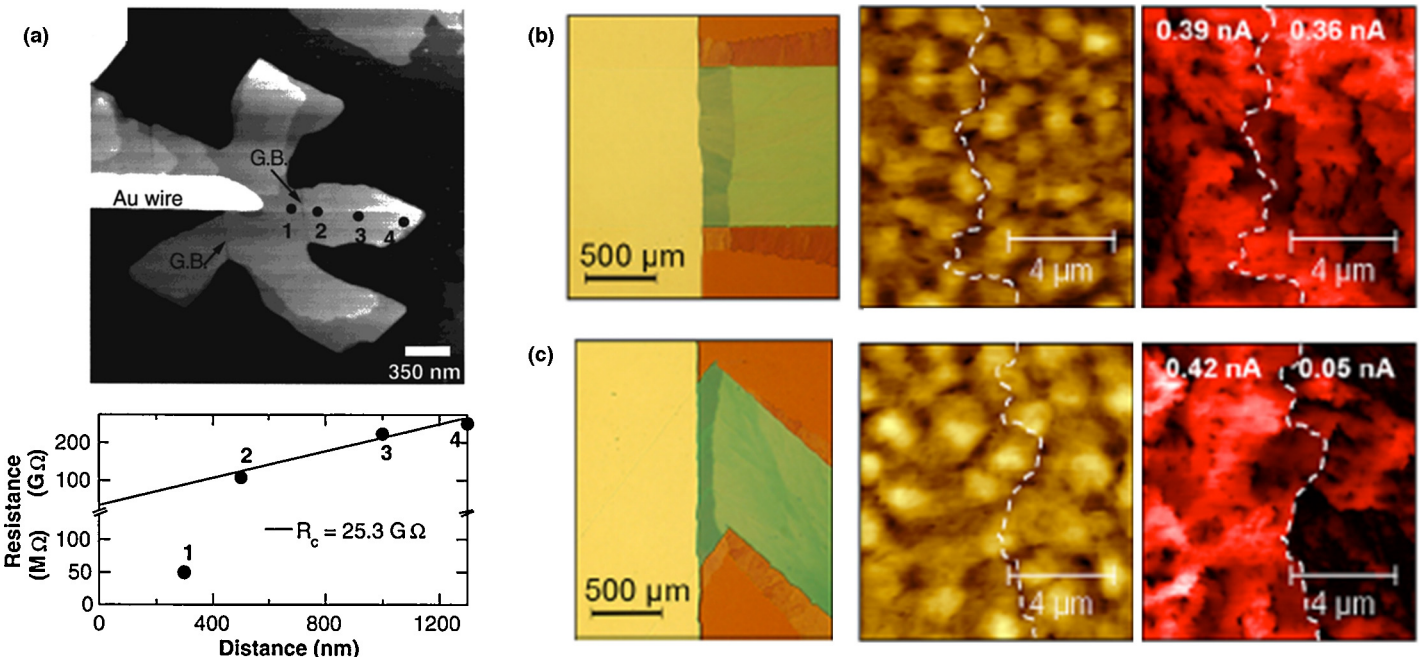

FIGURE 4

(a) Topography of a 6T crystal connected to a microfabricated Au wire on SiO_2, and plot reporting the resistance versus probe-wire separation distance, measured from local *I*–*V* on point marked as 1–4. The linear fit through points 2, 3, and 4 has been used to estimate the grain boundary resistance. Reproduced from [79] with the permission of Wiley-VCH. (b) and (c) Optical images, AFM topography images (*Z*-scale = 25 nm) and current maps (0–1.4 nA current scale) of (b) low-angle, and (c) wide-angle interspherulite boundaries in TES ADT polycrystalline films. Reproduced from [7] with the permission of ACS.

molecular orientation mismatch along their lengths. C-AFM revealed that current flow is unaffected when the mismatch of molecular orientation along a boundary is low (low-angle interspherulite boundaries, see Fig. 4b), while charge transport is limited by the presence of high-angle interspherulite boundaries (Fig. 4c) [7]. As a result, guiding crystallization in order to eliminate the presence of high-angle interspherulite boundaries was demonstrated to be a promising route toward the improvement of the overall organic thin-film transistor (OTFT) device performance [7].

The study of the electrical properties of individual nanostructures such as single fibers and wires has also represented a big challenge in the field of organic electronics, although it can be seen as just the first step toward the exploration of ensembles of nanostructures which communicate among each other with the ultimate goal of producing high performing device. The intrinsic electron mobility of individual N,N′-1H,1H-perfluorobutyldicyanoperylene-carboxydiimide PDIF-CN_2 supramolecular fibers was determined by three-terminal C-AFM to be $(1.5 \pm 0.8) \times 10^{-2}$ $cm^2\,V^{-1}\,s^{-1}$ under ambient conditions, being nearly three orders of magnitude higher than that of fiber ensembles [81]. Conversely, the longitudinal mobility μ_L on a single poly(3-alkylthiophene) nanofiber was estimated 0.07 ± 0.03 $cm^2\,V^{-1}\,s^{-1}$, differently from its transversal mobility μ_T of 10^{-5}–10^{-6} $cm^{-2}\,V^{-1}\,s^{-1}$. For one single nanofiber μ_T was found to decrease with increasing alkyl side chain length while μ_L was alkyl chain length independent [82]. Interestingly, the hole mobility of one fiber resulted to be similar to the mobility of a web of nanofibers; this finding was explained by the fact that the bridging of two or more individual nanofibers can be neglected with respect to the intrinsic resistance of the single nanofiber [83]. In 1996 for the first time the resistance of a single multiwall carbon nanotube of 14 nm diameter, physisorbed on an insulating SiO_2 substrate and contacted with a gold electrode, was measured by C-AFM [84]; by employing NbN coated tips as counter electrodes the estimated resistance amounted to 0.06 MΩ/μm. Later, the resistance of single wall carbon nanotubes (SWNT) was studied in detail in correlation to the presence of defects; it revealed that just a 0.03% of di-vacancies produces an increase of three orders of magnitude in the resistance of a SWNT of 400 nm length [85]. Beside organic polymer wires also metal–organic wires have been studied on the nanoscale [86,87]. The length dependent resistance measurements on metal–organic $[Pt_2(dta)_4I]_n$ (dta = dithioacetate) nanoribbons allowed the estimation of the distance between defects, finding that the inter-fiber transport is the limiting process in the crystals while transport along the single chains dominated in the nanoribbons [88].

One of the major questions to be addressed in C-AFM measurements of organic thin films and nanostructures is the maximum spatial resolution that can be achieved. Such a question is strictly related to the size of the contact, that is, how many molecules (or which sample area) are wired and thus explored on the same time during a data collection? A method allowing the control of the effective contact area could highly improve the interpretation of the data, especially when multicomponent blends, phase-segregated films or nanostructures are imaged. As an example, a variation of the effective contact area at the grain boundaries in polycrystalline films, could cause misinterpretation when showing an increase of the current at the edges. It will also be key to perform C-AFM in well-defined environments, not only to insulate the tip and sample from condensation of a water layer, but also to exploit well-defined gases to control reactivities.

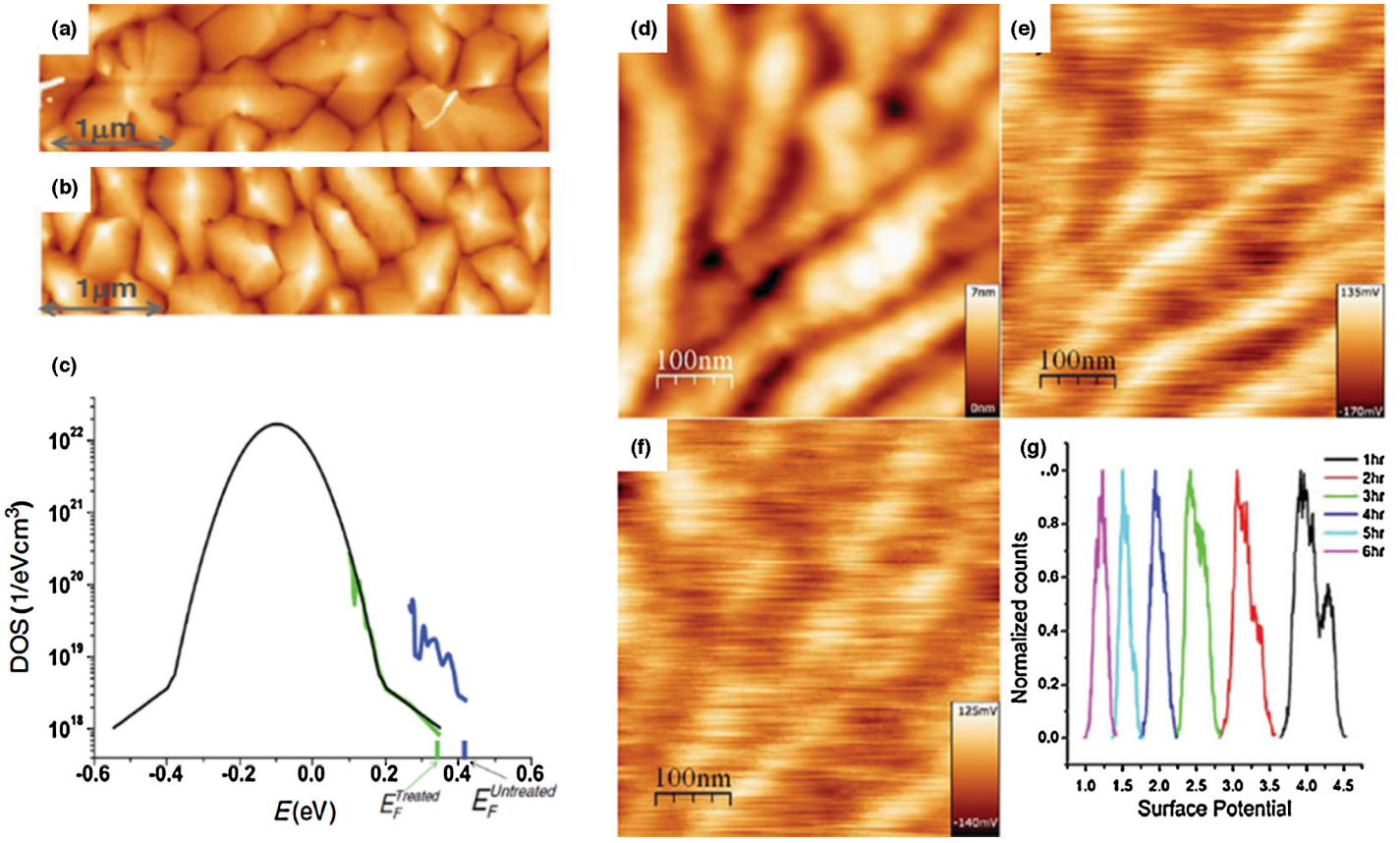

FIGURE 5

(a)–(c) Effect of HMDS treatment of the silicon oxide substrate on evaporated pentace thin film. AFM images acquire on (a) untreated and (b) treated substrate. (c) DOS spectrum extracted from the KPFM images on a working device. Reproduced from[95] with the permission of APS. (d)–(g) Effect of the bias stress on polymeric TFT. (d) AFM image, (e), (f) KPFM acquired at different times, and (g) the time-evolution of the surface potential distribution. Reproduced from [96] with the permission of APS.

In general, charge carrier injection and transport in disordered organic semiconductors are very different when compared with conventional inorganic semiconductors [89]. Being organic thin films often polycrystalline, the density and type of structural defects and grain boundaries strongly affect the charge transport and the key device parameters of TFT, such as effective charge mobility, threshold voltage, sub-threshold swing and electric stability during prolonged gate operation [90]. These structural defects are due to the formation of long-lived electronic states that trap charges at the interfaces between the electrodes, the gate dielectric and the organic semiconductor bulk film. Fermi level pinning due to the trap states transport in amorphous organic semiconductors is generally described in terms of charge-carrier hopping among disordered localized energy states [91]. Moreover, gap states can induce Fermi level pinning which has been observed for both small molecules and polymers [92,93].

The gap states in organic semiconductors have been measured by several experimental techniques such as photoconductivity, space-charge-limited current (SCLC), and electron spin resonance. Ultraviolet photoelectron spectroscopy (UPS) is the most common method to measure the whole spectrum of the electron density of states DOS on both inorganic and organic materials and has already been used for organic small molecules such as pentacene [94]. Yogev et al. [95] showed that the HMDS treatment of the SiO_2 substrate in TFT does not modify the surface morphologhy of the evaporated pentacene film (Fig. 5a,b) but it reduces of one order of magnitude the DOS of the trap states of the film respect to the untreated case (Fig. 5c). By using a KPFM-based method they monitored the Fermi level pinning for HMDS-treated sample by measuring the shift of the Fermi level, which results 70 meV closer to the HOMO band maximum in comparison to the untreated sample.

Defects play a fundamental role in the charge transport in highly conductive polymeric films. Poly[2,5-bis(3-alkylthiophen-2-yl)thieno (3,2-b)thiophene] (pBTTT) exhibited a field-effect mobility of 1 $cm^2 V^{-1} s^{-1}$ in devices likely because of the high order at the supramolecular level within the films, due to the interdigitation between polymer side chains. Yuen et al. [97] showed that the transport properties of thin films of doped pBTTT can be described as a one-dimensional ''metal'' (i.e. a Luttinger liquid) because tunneling is the dominant conduction mechanism through impurity/defect barriers within and between pBTTT chains, over a large range of temperatures, charge densities and applied voltages. Monitoring by AFM (Fig. 5d) and KPFM the potential of the polymeric network in the active layer of a transistor in the on-state at different times (Fig. 5e,f), Hallam et al. [96] showed that the disordered grain-boundary regions (ribbons) constitute preferential charge trapping sites and lead to significant lateral non-uniformity on a 100 nm length scale of the induced carrier concentration under accumulation conditions. In particular, KPFM images acquired at

different times show that the changing in the surface potential corresponding to the ribbons decays together with the average potential during device recovery, as shown by the SP distributions reported in Fig. 5g.

In the last decade we have witnessed the emergence of graphene as a material featuring unprecedented properties thereby holding potential to impact numerous areas of science and technology [98]. The outstanding electrical, optical, and mechanical properties of graphene make it a promising candidate for practical applications [99] in electronics [100–102], sensing [103,104], energy storage [105,106] and conversion [107]. In view of its zero band-gap, graphene cannot be directly used as active material in a field-effect transistor. An alternative strategy is to use oxygen-defect-rich graphene, that is, a water soluble monoatomic thick insulating layer known as graphene-oxide (GO) [108], and to reduce it reduced graphene-oxide (RGO) thereby rendering the film again electrically conducting. GO is a semi-amorphous material, where graphene-like sp^2 regions of very few nanometers width are embedded in a sp^3 matrix. Being the graphene like regions not in contact, GO is an electrical insulator. The maximum reduction yield provides to decrease the sp^3 bonded to approximately 20% of the carbon atoms so that transport in RGO occurs primarily by hopping rather than near ballistically, as in the case of mechanically exfoliated graphene [109].

Liscio et al. [110] blended RGO with poly(3-hexylthiophene) (P3HT) as the active layer of field-effect transistors. They showed devices exhibiting improved field-effect mobilities and as well as the I_{on}/I_{off} ratio. Mativetsky et al. [111] used C-AFM to reduce locally the GO films leading to conductive nanoscaled regions. The local reduction of GO film was induced by the charged C-AFM tip by exploiting the electrochemical decomposition of the water layer at the tip–GO interface. Mativetsky et al. [112] also demonstrated a new approach to fabricate graphene-based TFTs, starting from aqueous solutions of GO, processed entirely under ambient conditions. In this case both KPFM and C-AFM were used to monitor the electrical properties and the electrical potential decay directly on devices (Fig. 6) previously patterned with-selective deposition and reduction of GO sheets in between or on the surface of micro/nano-electrodes (Fig. 7).

In general, KPFM can be used to perform a not invasive test of organic materials in TFT, by mapping the electrical potential in a working device. Burgi et al. [113] produced a high-resolution map with 100 nm resolution of the electrostatic potential in the accumulation layer of P3HT TFTs, as well as investigated the time scale associated with charging or discharging the accumulation layer in TFTs based on P3HT. Nichols et al. [114] also used KPFM to simultaneously obtain high-resolution topography and potential images of pentacene OTFTs during device operation. Large potential drops at the source were observed. Puntambekar et al. [115] studied the potential drop between source and drain in top contact and bottom contact pentacene TFTs using KPFM. The potential drops were converted to resistances by dividing by the appropriate drain current values. It was found that the contact and the channel resistances decrease strongly with increasing gate bias, but do not depend strongly on the drain bias. These maps can be used to identify bottlenecks to charge transport and, in conjunction with simultaneous drain current measurements, allow resistance analysis of specific structures.

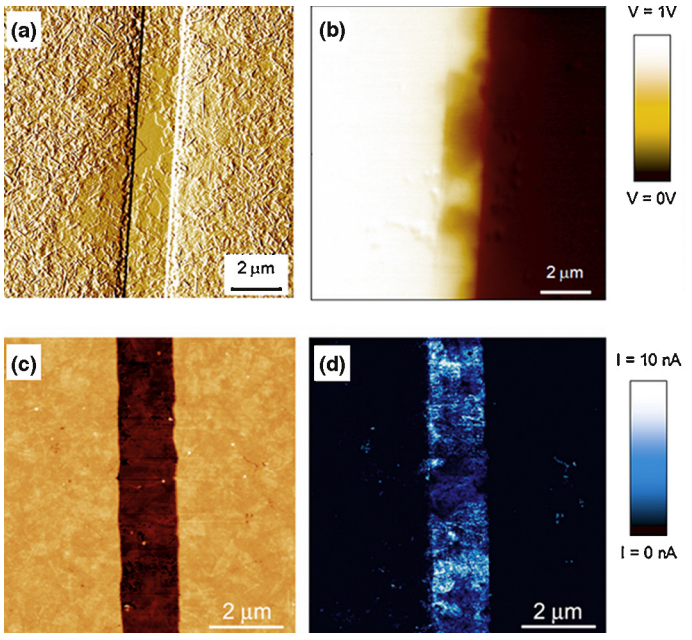

FIGURE 6

(a) AFM topography gradient image and (b) corresponding KPFM potential map acquired by applying a 1 V potential voltage to the left electrode while the right one is grounded. (c), (d) C-AFM current mapping of voltage-reduced GO in an FET channel. Simultaneously recorded (c) AFM topography and (d) current image of voltage-reduced GO between (unreduced) GO-covered Au electrodes. Reproduced from [112] with the permission of Wiley-VCH.

The shape of the KPFM tip plays a crucial role in the mapping the potential decay on working device. Even if the sharp tip apex allows to achieve a resolution of few tens of nm, the contribution of the cantilever cannot be neglected affecting the measured KPFM image with a broadening in potential in micron scale [24]. Thus, the correct estimation of the contribution of the cantilever

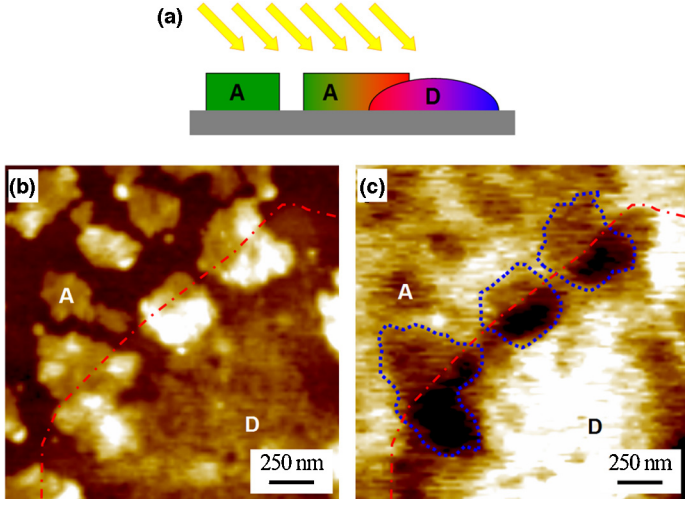

FIGURE 7

(a) Cartoon of illuminated sample showing both PDI electron accepting nanocrystals (A) in contact or not with amorphous aggregates of P3HT (D). (b) Topographical AFM image and (c) KPFM corresponding potential image recorded under illumination. Only the part PDI clusters physically in contact with P3HT are involved in the photocharge generation. *Z*-range: (b) 30 nm and (c) 90 mV.

becomes crucial for a quantitative measurement of the electrical potential along the TFT channel.

Organic blends for photovoltaics

Bulk hetero-junction (BHJ) are phase-segregated films obtained by co-deposition of an electron-donor and an electron-acceptor on a surface. The efficiency and the performance of a BHJ organic solar cell strongly depends on the connectivity and percolation of both the electron- and hole-transporting phases with their respective electrodes. In the recent years KPFM [116,117,118] and scanning tunneling spectroscopy (STS) [119] techniques are extensively used to directly observe the electrical potential along the charge transport paths of devices based on BHJ solar cells allowing to monitor dynamical production, transport and recombination of charges and therefore to correlate on the nanoscale the morphological properties with photogenerated charges and the with *I–V* characteristics of the device.

The morphology plays a paramount role in the percolation pathways for transport of both photogenerated excitons and charges. For this reason, alongside being able to study working electronic devices, C-AFM and KPFM are almost unique tools to study the organic blends under light stimuli and to correlate their morphological and electronic properties on the nanoscale, the typical scale of the diffusion lengths of the induced charges. Hoppe et al. [120] studied solid-state blends of poly[2-methoxy-5-(3,7-dimethyloctyloxy)]-1,4-phenylenevinylene (MDMO-PPV) and the soluble fullerene C60 derivative 1-(3-methoxycarbonyl) propyl-1-phenyl [6,6]C61 (PCBM), spin-cast from either toluene or chlorobenzene solutions. Experiments were performed either in the dark or under continuous-wave (CW) laser illumination at 442 nm. KPFM revealed distinct differences in the energetics on the surface of films cast from two solvents; by gathering complementary information by scanning electron microscopy, it was concluded that the films prepared from toluene solutions do not exhibit percolation pathways for electrons propagation toward the cathode. On the same system, Maturova et al. [121] measured a surface potential difference when sample is in the dark suggesting that holes diffuse from the PEDOT:PSS bottom contact into the polymer-rich phase. By illuminating the sample, the authors found a significant density of free photogenerated electrons in both the donor (polymer) and acceptor (fullerene) rich phases without a significant dependence on the length scale of phase separation. This finding suggests that the reduced performance of devices with coarse phase separation is at least partially due to a limited electron transport within the film.

Being bulk hetero-junctions three-dimensional systems, both the lateral and the vertical phase separations of the donor–acceptor blend device must be taken into account. Chiesa et al. [122] characterized the 3D structure of thin-film blends of poly-(9,9′-dioctylfluorene-co-benzothiadiazole) (F8BT) and poly-(9,9′-dioctylfluorene-co-bis-N,N′-(4-butylphenyl)-bis-N,N′-phenyl-1,4-phenylenediamine) (PFB) showing a complex morphology due to the different surface energy and solubility between the two polymers. The authors distinguished three regions: PFB-rich, ''bulk'' and ''interfacial'' F8BT-rich phases. By using monochromatic light (473 nm), the authors clearly observed that the F8BT boundary has a more negative potential than the bulk phase implying that part of the photogenerated charge does not recombine and remains trapped in the device under dark conditions. When the blend was illuminated, a negative shift of the surface potential was observed respect to the values measured in the dark. The importance of an efficient conduction path for photogenerated electrons to achieve a high device efficiency is clearly demonstrated by KPFM measurements showing that the highest surface photovoltage in the blend film is generated at the bilayer structures instead of the bulk one. Palermo et al. [123] showed that the mixing of long polymeric chains and highly crystalline assemblies of small polyaromatic molecules is a suitable strategy to maximize the density of these bilayer structures by reducing the phase separation and by increasing the donor–acceptor interpenetrated on the nanometer scale. In particular, they studied N,N″-bis(1-ethylpropyl)-3,4:9,10-perylenebis(dicarboximide) (PDI) and regioregular P3HT blends comparing the morphologies and the electronic properties at nanoscale with the device performances using i) monomeric PDI and ii) PDI-functionalized polyisocyanide.

By exploiting the lateral resolution of few tens of nm, KPFM provides a direct observation of the photogenerated excitons at the electron donor/acceptor interface. By using highly ordered nanoscopic crystals of 3″-methyl-4″-hexyl-2,2′:5′,2″:5″,2:5,2‴-quinquethiophene-1″,1″-dioxide (T5OHM, electron acceptor) embedded in a regioregular P3HT (electron donor) matrix and deposited onto ITO/PEDOT substrates, Palermo et al. [124] demonstrated that photogenerated excitons are split at the interface between the two materials, leading to the accumulation of electrons in the T5OHM crystals and holes in the P3HT polymer matrix. The difference between the average values of the surface potential of the two phases increases from 25 mV to more than 75 mV, allowing a much easier identification of the T5OHM crystals from the polymer matrix. The direct observation of the contact region between donor–acceptor material that results to be the only ''light active'' has been shown by Liscio et al. [125] through KPFM analysis of $CHCl_3$ cast N,N″-bis(1-ethylpropyl)-3,4:9,10-perylenebis(dicarboximide) (PDI) and regioregular P3HT blends. It was proved that only the PDI clusters that are in physical contact with P3HT exhibit an appreciable charge transfer because of the existence of a complementary electron donor phase. Upon illumination with white light, the surface potential of the P3HT phase became more positive and showed a value close to that of the substrate while PDI clusters in contact with P3HT became more negative. The measured potential variation induced by the light corresponds to a photo-induced charge density amounting to about 10^3 charges/μm^2.

In general, one of the reasons of the success of KPFM as a powerful tool to explore BHJ is given by its bulk sensitivity. Cadena et al. [126] directly showed the sub-surface sensitive of KPFM by imaging networks of single-walled nanotubes (SWNTs) dipped into a polyimide (PI) matrix. By devising a 3D model to single out the surface and the bulk contributions to the measured potential signal, Liscio et al. [127] described the sampling depth in terms of film electrical static permittivity, showing that on P3HT films the sub-surface sensitive of the technique amounts to about 100 nm. Nevertheless, a comprehensive model which takes into account the dielectric properties of the samples and the quasi-static electrical field is still lacking.

Nanoscale spatial variations in photocurrent across the surfaces of photovoltaic cells (OPVs) can be directly imaged while

irradiating the photosensitive material by PC-AFM (see Fig. 1c) [128–130]. By studying into details blends of poly(3-butylthiophene) nanowires as donors and $PC_{61}BM$ or $PC_{71}BM$ fullerenes as acceptors it was observed for example that efficient charge transport (high current in C-AFM images performed in dark) required a continuous pathway of one material through the film. In contrast, efficient photocurrent generation requires bi-continuous pathways of both materials. Films which may exhibit very high dark hole currents, polymer-rich surfaces, may not produce predominantly positive photocurrents evidencing a lack of a continuous fullerene pathway to the bottom electrode [131].

The evolution of the electronic properties with solvent–vapor annealing (SVA) of OPV was studied in polyfluorene–copolymer (poly(5,7-bis(3-dodecylthiophen-2-yl)thieno[3,4-b]pyrazine-alt-9,9-dioctyl-2,7-fluorene) (BTTP-F)) and PCBM blends, showing that SVA improved the power conversion efficiency by 40% while forming mesoscopic PCBM crystallites and a copolymer-rich overlayer at the cathode interface (Fig. 8) [8].

In a different approach, thiophene and fullerene moieties are present in the same donor–acceptor dyad in a poly(3-hexylthiophene) (P3HT) capped with [6,6]-phenyl-C61-butyric acid methyl ester (PCBM) polymer (PCB-c-P3HT) and it is the nanoscale structure and morphology of the polymer/fullerene interface which determine the photoinduced charge generation and the subsequent charge migration to electrodes. Nanospheres formed from THF solution show low dark current and photocurrent because both the PCB and P3HT portions of the dyad are isolated from the rest of the film, which decreases mobility and increases the recombination probability of charges. On the other hand, the crystallization of the P3HT core and alignment of the PCB of the dyad in wires from the *o*-DCB-cast film allows for high mobility and delocalization of charges, giving high dark current and photocurrent [132].

Electrical heterogeneity of the contacts can also play a significant role on the overall OPVs performance. A general approach for determination of the quality of electrical contact between electrodes and organic semiconductors (OSCs), on sub-micrometer to nanometer length scales has been reported by employing a copper phthalocyanine, CuPc donor layer deposited on a transparent ITO electrode modified with variable chain length alkyl-phosphonic acids (PAs). *I–V* curves were collected from an array of points of sub-100 nm lateral resolution, from which the hole mobility and the power dependence of the current–voltage behavior were extracted. A power dependence that deviates from 2 indicates the presence of a non-ohmic contact between the bottom electrode and the organic semiconductor. By correlating the injection efficiency of each site, measured as a deviation from an ohmic behavior, with the performance of organic photovoltaic cells (OPVs) based on CuPc/C60 heterojunctions built on these same ITO substrates, it was shown that the electrical heterogeneity in

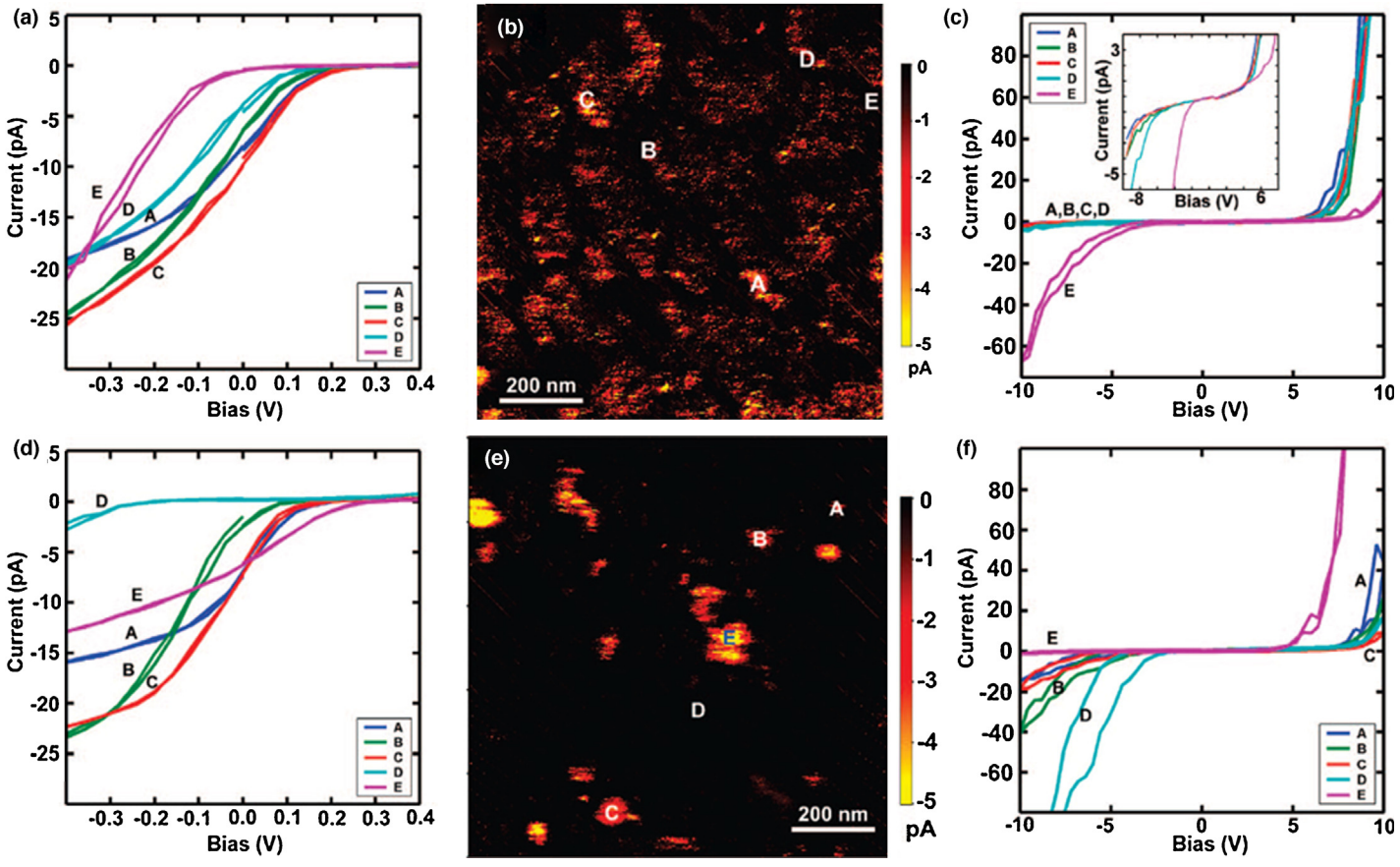

FIGURE 8

The evolution of the electronic properties with solvent-vapor annealing (SVA) of BTTP-F/PCBM blends OPV studied at the nanoscale by PC-AFM. Not-annealed film: (a) IV characteristics under 2 mW, 632 nm laser, (b) short circuit map, and (c) dark IV curves. Annealed film: (d) illuminated IV characteristics, (e) PC-AFM short-circuit map, and (f) dark IV curves. The local *I–V* curves (a), (c) and (d), (f) are performed on the points marked with capital letters on the maps (b) and (e), respectively. Reproduced from [8] with the permission of ACS.

the contact may play a key role in the overall device efficiency [133]. Since the morphology of BHJ is extremely complex, the performance of photovoltaic devices can be described as an inherently local property of the material. For this reason, both PC-AFM and KPFM are candidates to become routinely tools employed to quantitatively correlate the photo-charge generation with the phase segregated morphology, paving the way for a direct access to several mechanisms involved in the device as the charge generation, transport and the final collection at the electrodes. On this respect, also the use of light with different wavelengths and powers is mandatory in order to explore the electronic processes involved in a BHJ and their dynamics by tuning the excitation/de-excitation channels. KPFM could be extensively used to monitor the traps at the grain boundaries and inhomogeneities in the bulk material. A further point regards the tip used to probe the heterojunction. For example, by using C-AFM tip with different conductive coatings it could be possible to modulate the charge injection/extraction with sample tuning the measurement of the p/n channel. Furthermore, one has also to bear in mind that sharp metal tips under particular irradiation conditions can behave as metallic nano-antennas producing photoinduced electron emission [134]. This is actually not trivial to control but it should be considered for further development of the technique.

Conclusions

In summary, C-AFM and KPFM exhibit the unique capability of correlating structural and electronic properties in nanoscale architectures being important issues for both technological and scientific studies, since in electronic devices the performance is strongly dependent on the order at the supramolecular level. Because of this reason it is most likely that C-AFM and KPFM studies, as well as the combined use of both the techniques, can boost the optimization of the performance of organic electronic devices ultimately providing an important contribution to molecular, supramolecular and organic electronics.

In the last decade, AFM-based techniques went through major challenges based, among others, on the continuous improvement of the electronics. For example, the spatial resolution for long-ranged techniques such as KPFM was increased reaching atomic resolution for metals and ionic crystal [26]. Such a race toward reaching higher and higher spatial resolutions in KPFM is very risky: particular attention must be paid to avoid any cross-interference of the topography signal on the recorded surface potential signal. Beyond the spatial resolution, several other parameters have been improved such as faster scanning, performance in liquid environments or new detection modes. Typically, all AFM-based techniques feature a sub-millisecond time resolution, which is sufficient to explore charge trapping and de-trapping processes at the dielectric/semiconductor interface. A further enhancement of the time resolution will pave the way to study other phenomena such as the monitoring of the shallow traps that strongly affect the electrical performance of a device. Moreover, the development of both C-AFM [135] and KPFM [136] measurements in liquid environments will make it possible to enlarge the field of the applicability of these techniques (and all AFM-based ones in general) from the biology (living cells) to metallurgy (monitoring of wet oxidation processes). By enabling the quantitative mapping of interface energies at the solid–liquid interface, with a high spatial resolution, measurements in liquid could also provide a number of intriguing opportunities for application in surface science [137]. In these cases, the stability and the cleanness of the tip are strictly mandatory. A way to circumvent the problems can be to develop new detection AFM-based methods in order to maximize the suitable tip-sample interaction and to minimize all the others interactions that can affect the stability of the measurement. Being the tip-sample interaction a dynamical and complex system, a greater understanding will be surely achieved through the developments of models and viable computational procedures to extract quantitative information on the electrical and electronic properties of nanostructures. Overall, a bright future can be foreseen for these two methods, that most likely will become golden tools for scientists operating in the hot field at the cross-road between nanoscience and (opto)electronics.

Acknowledgements

This work was financially supported by the EC through the European Research Council project SUPRAFUNCTION (GA-257305), the Marie-Curie ITNs GENIUS (PITN-GA-2010-264694) and SUPERIOR (PITN-GA-2009-238177), the Graphene Flagship (GA-604391), and the International Center for Frontier Research in Chemistry (icFRC).

References

[1] A. Facchetti, Chem. Mater. 23 (3) (2011) 733.
[2] R.H. Friend, et al. Nature 397 (1999) 121.
[3] A.P. Kulkarni, et al. Chem. Mater. 16 (2004) 4556.
[4] S.R. Forrest, Nature 428 (2004) 911.
[5] S.S. Lee, Y.L. Loo, Annu. Rev. Chem. Biomol. Eng. 1 (2010) 59.
[6] V. Palermo, P. Samori, Angew. Chem. Int. Ed. 46 (24) (2007) 4428.
[7] S.S. Lee, et al. ACS Nano 6 (11) (2012) 9879.
[8] T.A. Bull, et al. ACS Nano 3 (3) (2009) 627.
[9] A.L. Briseno, et al. Nature 444 (7121) (2006) 913.
[10] C.J. Brabec, et al. Chem. Soc. Rev. 40 (3) (2011) 1185.
[11] G. De Luca, et al. Adv. Funct. Mater. 21 (7) (2011) 1279.
[12] A. Salleo, et al. Adv. Mater. 22 (34) (2010) 3812.
[13] J. Rivnay, et al. Chem. Rev. 112 (10) (2012) 5488.
[14] S. De Feyter, et al. Chem. Commun. (7) (2001) 585.
[15] P. Samori, J.P. Rabe, J. Phys. Condens. Mater. 14 (42) (2002) 9955.
[16] R. Berger, et al. Macromol. Rapid Commun. 30 (14) (2009) 1167.
[17] V. Palermo, et al. Chem. Commun. 32 (2007) 3326.
[18] P. Samori, J. Mater. Chem. 14 (9) (2004) 1353.
[19] J.M. Mativetsky, et al. Top. Curr. Chem. 285 (2008) 157.
[20] V. Palermo, et al. Adv. Mater. 18 (2) (2006) 145.
[21] M. Nonnenmacher, et al. Appl. Phys. Lett. 58 (25) (1991) 2921.
[22] S.A.L. Weber, et al. Nano Lett. 10 (4) (2010) 1194.
[23] C. Musumeci, et al. Nanoscale 5 (2013) 7756.
[24] A. Liscio, et al. Acc. Chem. Res. 43 (4) (2010) 541.
[25] T. Glatzel, et al. Appl. Surf. Sci. 210 (1–2) (2003) 84.
[26] W. Melitz, et al. Surf. Sci. Rep. 66 (1) (2011) 1.
[27] D.S.H. Charrier, et al. ACS Nano 2 (4) (2008) 622.
[28] G. Elias, et al. Beilstein J. Nanotechnol. 2 (2011) 252.
[29] D.M. Taylor, G.F. Bayes, Phys. Rev. E 49 (2) (1994) 1439.
[30] Y.X. Shen, et al. Rev. Sci. Instrum. 79 (2) (2008).
[31] J.C. Love, et al. Chem. Rev. 105 (4) (2005) 1103.
[32] I.H. Campbell, et al. Appl. Phys. Lett. 71 (24) (1997) 3528.
[33] M.P. Nikiforov, et al. Nano Lett. 8 (1) (2008) 110.
[34] D.M. Alloway, et al. J. Phys. Chem. B 107 (42) (2003) 11690.
[35] J. Lu, et al. Langmuir 15 (23) (1999) 8184.
[36] A. Liscio, ChemPhysChem 14 (6) (2013) 1283.
[37] A. Liscio, et al. Adv. Mater. 22 (44) (2010) 5018.
[38] D.J. Ellison, et al. Adv. Mater. 23 (4) (2011) 502.
[39] N. Saito, et al. Surf. Interf. Anal. 34 (1) (2002) 601.
[40] C.T. Tseng, et al. Appl. Phys. Lett. 91. (23) (2007).
[41] H.O. Finklea, et al. Langmuir 3 (3) (1987) 409.

[42] E. Sabatani, et al. J. Electroanal. Chem. 219 (1–2) (1987) 365.
[43] N. Crivillers, et al. Phys. Chem. Chem. Phys. 13 (32) (2011) 14302.
[44] N. Crivillers, et al. Adv. Mater. 25 (3) (2013) 432.
[45] N. Crivillers, et al. Adv. Mater. 23 (12) (2011) 1447.
[46] A. Virkar, et al. Adv. Funct. Mater. 19 (12) (2009) 1962.
[47] H.C. Yang, et al. J. Am. Chem. Soc. 127 (33) (2005) 11542.
[48] S.G.J. Mathijssen, et al. Adv. Mater. 20 (5) (2008) 975.
[49] D.J. Wold, C.D. Frisbie, J. Am. Chem. Soc. 122 (2000) 2970.
[50] D.J. Wold, et al. J. Phys. Chem. B 106 (11) (2002) 2813.
[51] S. Ho Choi, et al. Science 320 (5882) (2008) 1482.
[52] S. Ho Choi, et al. J. Am. Chem. Soc. 132 (2010) 4358.
[53] B. Kim, et al. J. Am. Chem. Soc. 133 (49) (2011) 19864.
[54] V.B. Engelkes, et al. J. Am. Chem. Soc. 126 (2004) 14287.
[55] S. Ho Choi, C.D. Frisbie, J. Am. Chem. Soc. 132 (2010) 16191.
[56] C. Musumeci, et al. Adv. Mater. 26 (2014) 1688.
[57] J.M. Mativetsky, et al. J. Am. Chem. Soc. 130 (2008) 9192.
[58] G. Ricœur, et al. J. Phys. Chem. C 116 (39) (2012) 20722.
[59] J. Beebe, et al. Phys. Rev. Lett. 97 (2) (2006).
[60] J.M. Beebe, et al. ACS Nano 2 (5) (2008) 827.
[61] K. Uchida, et al. J. Am. Chem. Soc. 133 (24) (2011) 9239.
[62] K. Smaali, et al. ACS Nano 4 (4) (2010) 2411.
[63] H. Song, et al. J. Am. Chem. Soc. 129 (2007) 3806.
[64] G. Wang, et al. J. Am. Chem. Soc. 131 (2009) 5980.
[65] X.D. Cui, et al. Science 294 (5542) (2001) 571.
[66] S.V. Aradhya, et al. Nat. Mater. 11 (2012) 872.
[67] M. Frei, et al. Nano Lett. 11 (4) (2011) 1518.
[68] M. Kamenetska, et al. J. Am. Chem. Soc. 132 (2010) 6817.
[69] B. Xu, et al. J. Am. Chem. Soc. 125 (2003) 16164.
[70] K. Smaali, et al. ACS Nano 6 (6) (2012) 4639.
[71] C.M. Guédon, et al. Nat. Nanotechnol. 7 (2012) 305.
[72] V.B. Engelkes, et al. J. Phys. Chem. B 109 (2005) 16801.
[73] G.V. Dubacheva, et al. Small 10 (3) (2014) 454.
[74] B.L. Hendriksen, et al. Nano Lett. 11 (10) (2011) 4107.
[75] M.J. Loiacono, et al. J. Phys. Chem. B 102 (1998) 1679.
[76] E.L. Granstrom, C.D. Frisbie, J. Phys. Chem. B 103 (1999) 8842.
[77] T.W. Kelley, C.D. Frisbie, J. Vac. Sci. Technol. B: Microelectron. Nanomet. Struct. 18 (2) (2000) 632.
[78] T.W. Kelley, C.D. Frisbie, J. Phys. Chem. B 105 (2001) 4538.
[79] T.W. Kelley, et al. Adv. Mater. 11 (3) (1999) 261.
[80] A.B. Chwang, C.D. Frisbie, J. Appl. Phys. 90 (3) (2001) 1342.
[81] J.M. Mativetsky, et al. Adv. Mater. 26 (2014) 430.
[82] J.-C. Bolsée, et al. Org. Elect. 12 (12) (2011) 2084.
[83] J.-C. Bolsée, et al. Adv. Funct. Mater. 23 (7) (2013) 862.
[84] H. Dai, et al. Science 272 (1996) 523.
[85] C. Gomez-Navarro, et al. Nat. Mater. 4 (7) (2005) 534.
[86] L. Welte, et al. Nat. Nanotechnol. 5 (2010) 111.
[87] J. Gómez-Herrero, F. Zamora, Adv. Mater. 23 (44) (2011) 5311.
[88] C. Hermosa, et al. Nat. Commun. 4 (2013) 1709.
[89] S. Barth, et al. Phys. Rev. B 60 (12) (1999) 8791.
[90] A. Salleo, et al. Appl. Phys. Lett. 86 (26) (2005).
[91] H. Bassler, Phys. Status Solidi B Basic Res. 175 (1) (1993) 15.
[92] D.A. Evans, et al. Appl. Surf. Sci. 212 (2003) 417.
[93] C. Tengstedt, et al. Appl. Phys. Lett. 88 (5) (2006).
[94] H. Fukagawa, et al. Phys. Rev. B 73 (24.) (2006).
[95] S. Yogev, et al. Phys. Rev. B 84 (16.) (2011).
[96] T. Hallam, et al. Phys. Rev. Lett. 103 (25.) (2009).
[97] J.D. Yuen, et al. Nat. Mater. 8 (7) (2009) 572.
[98] K.S. Novoselov, et al. Science 306 (5696) (2004) 666.
[99] K.S. Novoselov, et al. Nature 490 (7419) (2012) 192.
[100] K.S. Novoselov, et al. Nature 438 (7065) (2005) 197.
[101] R.M. Westervelt, Science 320 (5874) (2008) 324.
[102] C.A. Palma, P. Samori, Nat. Chem. 3 (6) (2011) 431.
[103] F. Schedin, et al. Nat. Mater. 6 (9) (2007) 652.
[104] V. Dua, et al. Angew. Chem. Int. Ed. 49 (12) (2010) 2154.
[105] M. Pumera, Energy Environ. Sci. 4 (3) (2011) 668.
[106] Y.Q. Sun, et al. Energy Environ. Sci. 4 (4) (2011) 1113.
[107] M.D. Stoller, et al. Nano Lett. 8 (10) (2008) 3498.
[108] D.R. Dreyer, et al. Chem. Soc. Rev. 39 (1) (2010) 228.
[109] A. Bagri, et al. Nat. Chem. 2 (7) (2010) 581.
[110] A. Liscio, et al. J. Mater. Chem. 21 (9) (2011) 2924.
[111] J.M. Mativetsky, et al. J. Am. Chem. Soc. 132 (40) (2010) 14130.
[112] J.M. Mativetsky, et al. J. Am. Chem. Soc. 133 (36) (2011) 14320.
[113] L. Burgi, et al. Appl. Phys. Lett. 80 (16) (2002) 2913.
[114] J.A. Nichols, et al. Appl. Phys. Lett. 83 (12) (2003) 2366.
[115] K. Puntambekar, et al. Adv. Funct. Mater. 16 (7) (2006) 879.
[116] J. Lee, et al. Appl. Phys. Lett. 99 (24) (2011).
[117] R. Saive, et al. Appl. Phys. Lett. 103 (24.) (2013).
[118] R. Saive, et al. Adv. Funct. Mater. 23 (47) (2013) 5854.
[119] M.C. Shih, et al. Nano Lett. 13 (6) (2013) 2387.
[120] H. Hoppe, et al. Adv. Funct. Mater. 14 (10) (2004) 1005.
[121] K. Maturova, et al. Adv. Funct. Mater. 19 (9) (2009) 1379.
[122] M. Chiesa, et al. Nano Lett. 5 (4) (2005) 559.
[123] V. Palermo, et al. J. Am. Chem. Soc. 130 (44) (2008) 14605.
[124] V. Palermo, et al. Adv. Funct. Mater. 17 (3) (2007) 472.
[125] A. Liscio, et al. J. Am. Chem. Soc. 130 (3) (2008) 780.
[126] M.J. Cadena, et al. Nanotechnology 24 (13) (2013).
[127] A. Liscio, et al. Small 7 (5) (2011) 634.
[128] C. Groves, et al. Acc. Chem. Res. 43 (5) (2010) 612.
[129] R. Giridharagopal, et al. Mater. Today 13 (8) (2010) 50.
[130] D.C. Coffey, et al. Nano Lett. 7 (3) (2007) 738.
[131] H. Xin, et al. ACS Nano 4 (4) (2010) 1861.
[132] D.A. Kamkar, et al. ACS Nano 6 (2) (2012) 1149.
[133] G.A. MacDonald, et al. ACS Nano 6 (11) (2012) 9623.
[134] C. Ropers, et al. Phys. Rev. Lett. 98 (4.) (2007).
[135] N.N. Gosvami, et al. J. Phys. Chem. C 112 (1) (2008) 297.
[136] N. Kobayashi, et al. J. Appl. Phys. 110 (4.) (2011).
[137] A. Ruediger, F. Rosei, Nat. Nanotechnol. 5 (6) (2010) 388.